Measurement of the pressure distribution on a circular cylinder

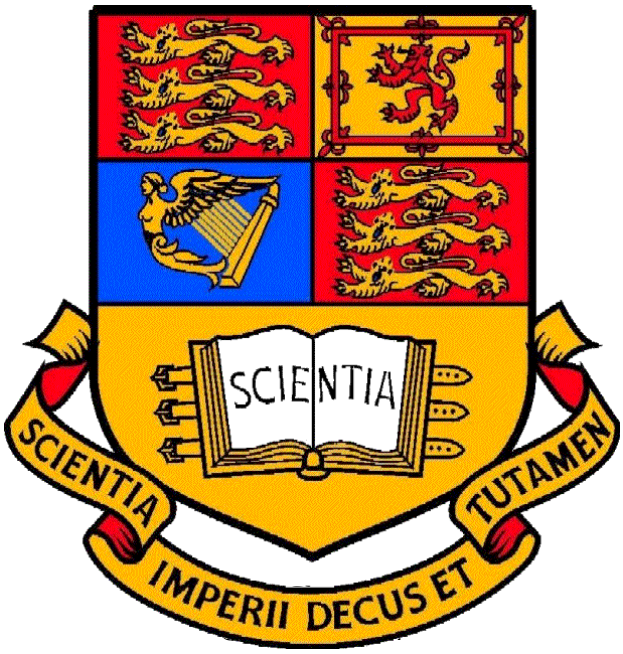

Submission Date: 26th November 2018

Xerxes Chong Xian

Submission Date: 26 November 2018

Abstract

The potential flow theory states that the drag experienced by a body moving at constant velocity is zero, under the assumption the fluid is incompressible, inviscid and irrotational. However, the theory does not account for viscous effects present, which dominate within the boundary layer. It wasn't until 1904 did Ludwig Prantl prove that viscous effects resulted in drag on bodies. In this experiment, a stationary circular cylinder is tested in flows of different Reynolds numbers. The use of a tripwire to trip the flow prior to the laminar separation point allows analysis of the effects of boundary layer transition from laminar to turbulent. The results show that the cylinder does experience drag, with pressure drag dominating the drag production due to the wake. A turbulent boundary layer also decreases the resultant drag by as much as 50% as the separation point shifts about 25° downstream from its un-tripped location.

Table of Contents

Definitions

$C'_D : Uncorrected\ Coefficient\ of\ Drag$

$C_D : Corrected\ Coefficient\ of\ Drag$

$C'_P : Uncorrected\ Coefficient\ of\ Pressure$

$C_P : Corrected\ Coefficient\ of\ Pressure$

$Re : Reynolds\ Number$

$Re_{Crit} : Critical\ Reynolds\ Number$

$\theta : Angle\ measured\ in\ degrees\ from\ the\ forward\ stagnation\ point\ at\ 0^{\circ}$

Introduction

A cylinder of diameter 0.102m is tested in a wind tunnel of height 0.46m at 2 speeds. At each speed, it is tested in a tripped and un-tripped condition. In this report, the graphs of pressure distributions measured as C_P , obtained from tappings along the upper surface of the cylinder will be plotted against their locations θ, measured in degrees from the forward stagnation point at $\theta = 0°$. From here, the changes in coefficients of pressure along the surface under different flow conditions are observed and discussed. After accounting for the blockage effects and applying a numerical integration method, the coefficients of lifts and drags for the cylinder are obtained, where the effects of boundary layer transition on drag production are also discussed.

Background

Potential flow theory is a model of fluid dynamics that works for incompressible, irrotational and inviscid flows. From the conditions of incompressibility and irrotationality, the stream function and the velocity potential can be shown to satisfy the Laplace Equation. Using the principle of superposition, the velocity potential for a circular cylinder in a uniform stream can be found. Combining Bernoulli's Equations with the definition of C_P, the theoretical C_P along a circular cylinder with respect to the angle θ, is defined as: $C_P = 1 - 4\,sin^2\,\theta$ (1)

This equation describes axisymmetric flow around the cylinder, with stagnation points located at $\theta = 0°$ and $\theta = 180°$ and maximum velocity at $\theta = 90°$ and $\theta = 270°$. This led to the famous D'Alambert Paradox, which indicated zero drag and zero lift generated as the flows is symmetric about both axes. However, in real and viscid flows, viscous forces dominate the flow in the boundary layer along the surface. As the flow follows the curvature of the cylinder, it slows downs due to the no slip condition. This deceleration of the flow along the curvature of the cylinder causes pressure to increase along the surface. Known as an adverse pressure gradient, it causes separation when the flow is eventually brought to rest by the no slip condition.

Potential flow theory is limited by its failure to model flow over bluff bodies as it does not account for flow separation that occurs in real, viscid flows, leading to the paradox. However, it is useful when combined with an appropriate conformal transformation to convert the flow over a circular cylinder to flow over aerofoil shapes to obtain good approximations of lift and drag.

Blockage effects were present in this experiment. This effect is an increase in test-section velocity caused by the reduced cross-sectional area due to the presence of the bluff body. Using Bernoulli's Equation and assuming mass continuity, this results in a lower static pressure and higher flow velocities in the test section (2). Using the formula for the blockage ratio found in the formula table in Table 3: Other variables and constant used for calculations in the report

Appendix B, a ratio of 0.22 was calculated. This exceeds the limit of 0.03 given in (2), hence the correction equations by Allen and Vincenti found in (3) were applied.

Results

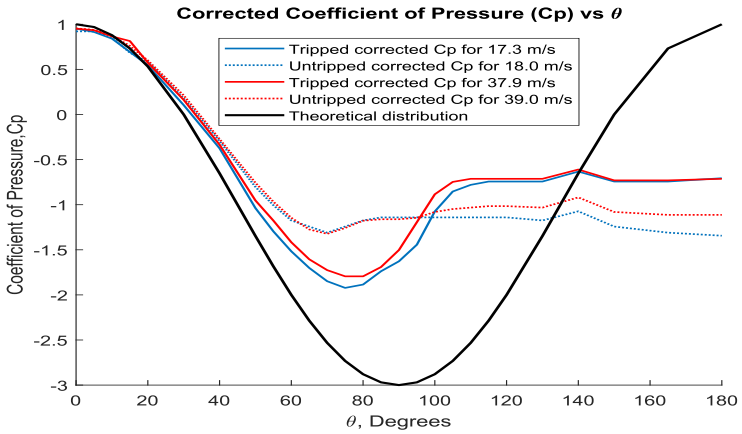

Figure 1. Corrected C_p distributions are plotted against θ with theoretical values for comparison.

From Figure 1, the tripped cases generated lower C_P compared to the un-tripped cases from between the angles of 0° to about 105°. From 105° to 180°, the tripped cases then started generating higher C_P than un-tripped cases. These results are in line with those in found in Figure 5 in Appendix C. The angle beyond which the C_P values start to become constant corresponds to the separation point, which is approximately 80° in the un-tripped cases and 105° in the tripped cases. This demonstrates the movement of the separation point downstream with a tripped flow.

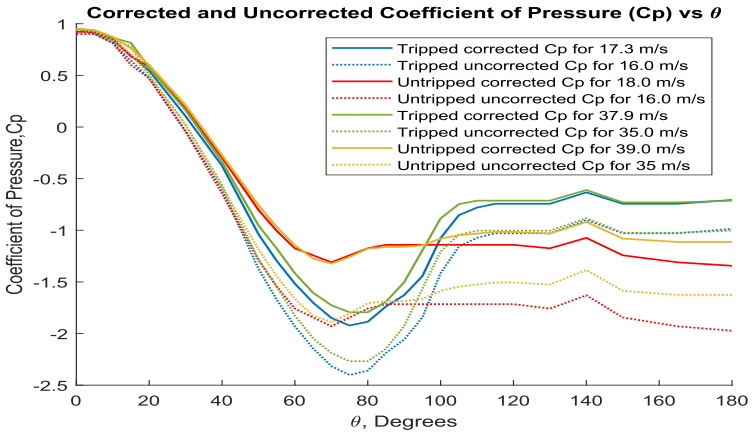

Figure 2. Plotting the corrected and uncorrected data shows the effect of corrections.

Figure 2 illustrates the effect of the correction equations applied. The corrected C_P values are higher than the uncorrected C_P values for all test cases. The corrected velocities have also been displayed. The corrected velocities are higher due to the blockage effects, leading to larger C_P values.

	Coefficients of Drag (C_D)				Coefficients of Lift (C_L)			
Velocities	**16 m/s**		**35 m/s**		**16 m/s**		**35 m/s**	
Flow Setup	**Tripped**	**Un-tripped**	**Tripped**	**Un-tripped**	**Tripped**	**Un-tripped**	**Tripped**	**Un-tripped**
Uncorrected	0.70	1.55	0.74	1.34	-1.32	-1.48	-1.24	-1.36
Corrected	0.60	1.22	0.64	1.08	-0.99	-0.96	-0.91	-0.90
Direct Correction	0.56	1.09	0.59	0.98	–	–	–	–

Table 1. Table of corrected and uncorrected values of C_D & C_L for the 4 test cases. No direct correction was available for C_L.

From Table 1, it is evident that tripping the boundary layer reduces the amount of drag produced. This is seen by much lower C_D values measured in the tripped cases, with values more than halving in some cases. The direct correction method gives the lowest values of C_D. Comparing the uncorrected and corrected values, the blockage effect increases C_D. Using pressure readings for only the top-half the cylinder surface, the application of the C_L formula in the Appendix B, yielded non-zero values. Assuming an axisymmetric flow, with an equal number of pressure readings on the bottom-half of the cylinder yielding the same pressure readings, the C_L formula would yield values of the order 10^{-16}, approximately zero. This supports the theory that axisymmetric flows generate no lift.

Discussion

As seen from Figure 1, is it evident that the separation has shifted downstream with a transition from laminar to turbulent flow. The local turbulent flow aft the trip wire had re-energised the separated flow and it reattached to the cylinder as a turbulent boundary layer, forming a separation bubble (2). The turbulent boundary layer has a higher momentum, overcoming the adverse pressure gradient for longer but eventually separates further downstream, creating a smaller wake. A smaller wake area results in a net lower pressure drag, leading to a lower drag coefficient. Although the turbulent flow

also increases the skin friction produced, pressure drag is a larger contributor to total drag than skin friction for bluff bodies (4), hence the total drag decreases.

The drag crisis phenomenon is widely known and has been exploited in various applications. The patterned dimples of a golf ball create a thin turbulent boundary layer that delays flow separation, reducing overall drag, allowing the golf ball to fly further and straighter than a smooth sphere. The stitches, their orientation and surface roughness found on baseballs also promote transition. When combined with additional spin (generating circulation) by a skilled player, complex lift and drag distributions are created than enables the player to change the ball's trajectory.

The pressure readings were determined by the ethanol height in the manometer, which were dependent on the static pressure tappings on the cylinder surface. At lower flow velocities, the pressure and height variations will not be as pronounced compared to higher velocities, where static pressure is lower. Testing at higher flow speeds would have increased the reliability of the results.

The flow characteristics around a cylinder changes with an increasing Re. To visualise the flow changes, Figure 8.13 on Page 503 from (5) is referenced here. The points (a,b,c,d,e,f) make reference to the respective diagrams in the figure. The figure can be found in Figure 3 of Appendix C.

a) Streamlines are nearly symmetrical; the flow is attached. Known as Stokes Flow, it gets increasingly asymmetric upstream and downstream of the cylinder as Re increases.
b) From Re of 5 to 40, the flow separates from the rear of the cylinder to form a recirculating wake, which grows in length as the Re increases further.
c) The recirculating wake becomes gradually unstable due to small disturbances, developing vortices that are shed periodically on alternate sides of the cylinder, forming a row of vortices. This phenomenon is known as the Kármán Vortex Street.
d) As the Re increases, the vortex sheet becomes increasingly turbulent, becoming a pronounced wake. the separation point from occurs around the point of maximum thickness. The C_D is relatively constant till a Re of about 3.0×10^5.
e) A further increase in Re promotes transition of the boundary layer from laminar to turbulent as it separates. This turbulent layer re-energises the flow and causes it to reattach to the surface, creating a separation bubble (2) and a smaller wake. The resultant in C_D is called a drag crisis. It proceeds to travel further down the contour before separating again.
f) Beyond a Re of 3.0×10^6, the boundary layer transits directly to turbulent flow without prior separation. The wake begins to widen, with consequent increase in C_D as the separation points move up. This point is known as the Critical Reynold's Number (Re_{crit})

Though the Re could have been varied by altering the diameter of the cylinder, the pressure of the air and even its viscosity, it is much simpler and direct to control the velocity of the flow to alter the Re. While increasing the velocity will increase the Re of the flow, the desired range of higher Re are not attainable even the wind tunnels maximum operating power. Hence a tripwire was utilised to trip the flow, promoting an early transition from laminar to turbulent flow, thereby increasing the Re.

For the directly corrected C_D values of 0.56 and 0.59 of the tripped cases conducted at 16m/s and 35m/s, its Re using the formula found in Appendix B, are 1.1×10^5 and 2.4×10^5. This indicates an increase in C_D with an increase in Re. Theoretically, such an increase with a turbulent boundary layer would lie within the super critical regime of Re, beyond Re_{crit}. An observation of Figure 6 from Appendix C shows that a Re range of 1.1×10^5 to 2.4×10^5, does not correspond to the supercritical regime of the graph. Hence, we can conclude that the graph of C_D against Re for the circular cylinder has "shifted" to the left when the boundary layer is tripped. An example of such shifting can be seen in Figure from Appendix C.

The equivalent Re for these C_D values obtained from Figure 6 in Appendix C would be around 2.0×10^6, with the C_D values of 0.59 having a higher Re. These Re are an entire order of 10^1 larger than the calculated values.

Sources of error

The blockage effect increases the coefficient of pressure and decreases the drag on the cylinder. Since the properties of the flow are altered, the behaviour of the flow and the wake will be altered. Correction equations used do not consider the interference effects from the separation mechanism of the wake and the structure of the wake behind the body. These effects are prominent in regions where C_D changes rapidly with Re. (3)

Other possible errors include the instability of the wind velocity values displayed by the wind tunnel controls as well as the fluctuation of the ethanol height on the manometer. The manometer was also tilted at angles of $20°$ and $50°$ with no reliable way to confirm its accuracy. The C_D were obtained using the trapezoidal numerical integration method in MatLab, where the C_P was obtained from pressure tappings space at intervals between $5°$ and $15°$. The accuracy of the experiment could have been increased with a larger number of tappings spaced evenly along the cylinder surface.

Conclusion

This experiment has successfully demonstrated that a body moving at constant velocity experiences drag, contradicting the zero-drag prediction from potential flow theory. It has provided insight into the mechanisms behind the drag crises, showing that a transition to turbulent flow delays flow separation, reduces the wake size and thus reduces drag. The drag crisis also verifies that pressure drag dominates drag forces on bluff bodies and it can be exploited by means of promoting boundary layer transition to turbulent flow. The impact of the blockage effect is evident in the uncorrected and corrected data, making it an important consideration in wind tunnel testing. Despite corrections, it is necessary to be aware of the corrections limitations and the contribution of other sources of errors.

Bibliography

1. **Anderson, JD.** *Fundamental of Aerodynamics, 5th Edition.* s.l. : McGraw-Hill Higher Education, 2011.
2. **P. Cosyn, D. Olivari, D. Portugaels.** *Drag Coefficient Determination of Bluff Bodies - Analysis of Blockage Effects.* Rhode Saint Genèse, Belgium : Von Karman Institute for Fluid Dynamics, 2004.
3. **Roshko, Anatol.** *Experiments on the flow past a circular cylinder at very high Reynolds Number.* Pasadena, California : Guggenheim Aeronautical Laboratory, California Institute of Technology, 1960.
4. *Drag and Wake Modification of Axisymmetric Bluff Bodies Using Coanda Blowing.* **Freund, J.B & Mungal, M.G.** Stanford, California : Stanford University, 1994, Journal of Aircraft.
5. **Houghton, E. L., et al.** *Aerodynamics for Engineering Students, Sixth Edition.* Oxford : Elsevier, 2013. pp. 502-504.
6. *Mechanism of drag reduction for circular cylinders with patterned surface.* **Butt, U., L, Jehring and Egbers, C.** s.l. : Elsevier, February 2014, International Journal of Heat and Fluid Flow, Vol. 45.

Appendix A
Unprocessed Data and Other Variables

		Manometer Uncorrected Pressure heights (in)			
Test Velocity (m/s)		16		35	
Tapping Number	Angle (°)	Tripped	Un-tripped	Tripped	Un-tripped
1	-30	10.9	10.5	11.1	10.3
2	0	8.6	8.3	6.4	5.9
3	5	8.7	8.3	6.5	6
4	10	8.9	8.5	6.9	6.4
5	15	9.3	9	7.2	7.1
6	20	9.7	9.3	8.6	8.1
7	30	10.9	10.5	11.0	10.5
8	40	12.2	11.9	13.9	13.5
9	50	14.0	13.4	17.5	16.5
10	55	14.7	14.0	18.8	17.8
11	60	15.3	14.5	20.2	18.9
12	65	15.8	14.7	21.3	19.7
13	70	16.2	14.9	22.0	20.0
14	75	16.4	14.7	21.3	19.7
15	80	16.3	14.5	22.4	19.1
16	85	15.9	14.4	21.8	19.0
17	90	15.6	14.4	20.7	19.0
18	95	15.1	14.4	18.9	18.9
19	100	14.1	14.4	17.1	18.5
20	105	13.5	14.4	16.3	18.3
21	110	13.3	14.4	16.1	18.2
22	115	13.2	14.4	16.1	18.1
23	120	13.2	14.4	16.1	18.1
24	130	13.2	14.5	16.1	18.2
25	140	12.9	14.2	15.5	17.5
26	150	13.2	14.7	16.2	18.5
27	165	13.2	14.9	16.2	18.7
28	180	13.1	15.0	16.1	18.7

Table 2: Ethanol pressure heights from the manometer

Other Test Variables					
Test Velocity (m/s)		16		35	
Manometer Angle (°)		20	20	50	50
Room Temperature (°C)		17.4	17.5	19.8	19.5
Room Pressure (kPa)		101.70	101.75	101.75	101.75
Ethanol Density (kg/m^3)		789	789	789	789
Air	Density (kg/m^3)	1.225	1.225	1.225	1.225
	Dynamic Viscosity (kg/m^2s)	1.83×10^{-5}	1.83×10^{-5}	1.83×10^{-5}	1.83×10^{-5}

Table 3: Other variables and constant used for calculations in the report

Appendix B
Formula Table

Coefficient of Drag	$C_D = \int_0^{\pi} C_P \cos\theta \ d\theta$ Solved using a numerical integration method
Coefficient of Lift	$C_L = \frac{1}{2}\int_0^{2\pi} C_P \sin\theta \ d\theta$ Solved using a numerical integration method
Theoretical Coefficient of Pressure (Potential Flow Theory)	$C_P = 1 - 4\sin^2\theta$
Coefficient of Pressure (Pressure tapping)	$C_P = \frac{P - P_s}{\frac{1}{2}\rho U^2}$ $U : Flow\ Velocity$ $P_s : Free\ stream\ static\ pressure$ $P : Pressure\ tapping\ reading$
$Reynolds\ Number$	$Re = \frac{\rho U d}{\mu}$ $\rho : Air\ density$ $U : Flow\ Velocity$ $d : Diameter\ of\ cylinder$ $\mu : Dynmic\ Viscosity$
Velocity Correction (3)	$\frac{V}{V'} = 1 + 0.25C'_D\left(\frac{d}{h}\right) + 0.82(\frac{d}{h})^2$ $V' : Uncorrected\ Velocity$ $V : Corrected\ Velocity$ $C'_D : Uncorrected\ Coefficient\ of\ Drag$
Coefficient of Drag Correction (3)	$\frac{C_D}{C'_D} = 1 - 0.5C'_d\left(\frac{d}{h}\right) + 2.5(\frac{d}{h})^2$ $C'_D : Uncorrected\ Coefficient\ of\ Drag$ $C_D : Corrected\ Coefficient\ of\ Drag$
Coefficient of Pressure Correction (3)	$C_P - 1 = \left(\frac{V'}{V}\right)^2 (C'_P - 1)$ $C'_P : Uncorrected\ Coefficient\ of\ Pressure$ $C_P : Corrected\ Coefficient\ of\ Pressure$
Blockage Ratio	$\frac{d}{h}$

	d : *Diameter of cylinder* h : *Height of wind tunnel* Correction equations to be applied when blockage ratio exceeds 0.03 (2)

Table 4: Table of the key equations used in this report

Appendix C
Diagrams

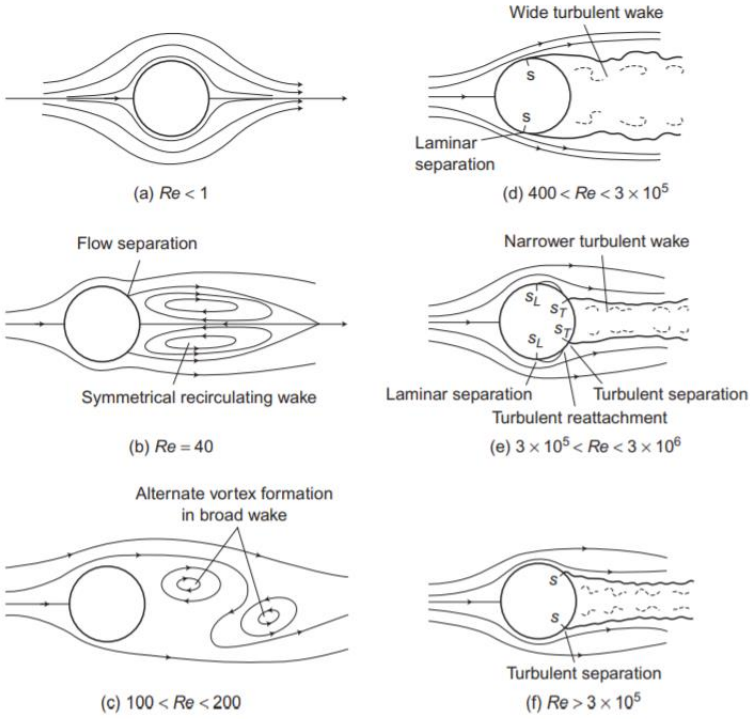

Figure 3. Sketches of the changing flow characteristics (4)

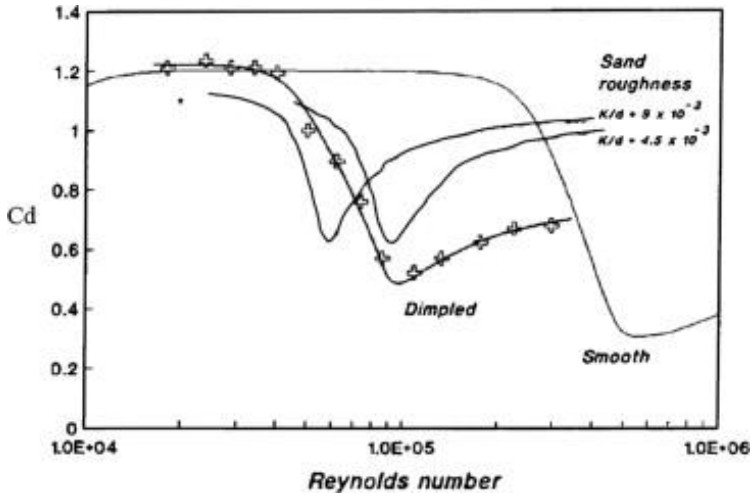

Figure 4. An example of the graph of C_D vs Re shifting to the left with increasing roughness (6)

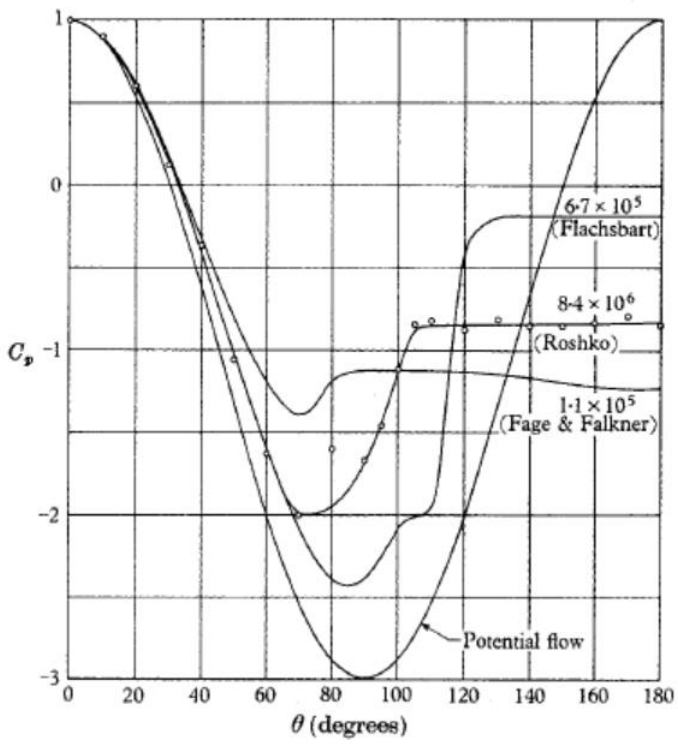

Figure 5. Experimental and theoretical variation of C_P with θ from Roshko (3)

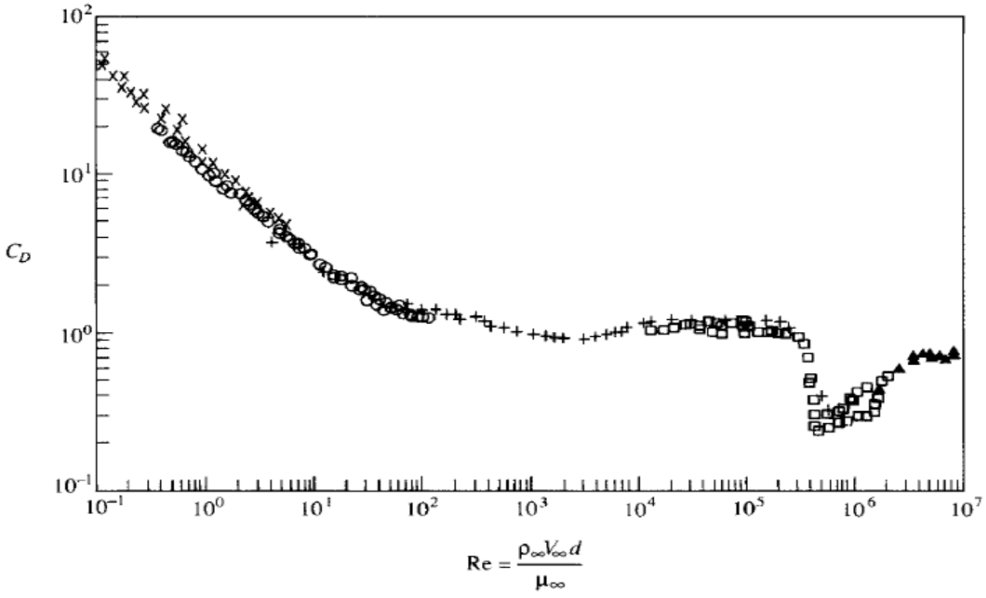

Figure 6. Variation of cylinder-drag coefficient with Reynolds Number (1)

Appendix D
MatLab Script

A 157-line Matlab script was used to process the raw data above. The Trapezoidal numerical integration method was applied using the trapz function in Matlab.

```
clear
clc

%constants
d=0.102;
h=0.46;
Uinf=[16 16 35 35];
inch2m=0.0254;
rhoair=1.225;
rhoethanol=789;
g=9.81;
mui=1.825*(10^-5);
alpha=[20,50];
totalheight=[8.5,8.1,6.4,5.8];
atm=[101700,101750,101750,101750];
%Extract data from excel, correct pressure heights with alpha
(viewing
%angle)
data1=xlsread('Cylinder Data and
Calculations.xlsm','Sheet1','D6:K32');
data2=xlsread('Cylinder Data and
Calculations.xlsm','Sheet1','A6:A32');
theta=deg2rad(data2);
Pressureheight=zeros(27,4);
Pressureheight(:,1)=inch2m*sind(alpha(1))*data1(:,1);
Pressureheight(:,2)=inch2m*sind(alpha(1))*data1(:,3);
Pressureheight(:,3)=inch2m*sind(alpha(2))*data1(:,5);
Pressureheight(:,4)=inch2m*sind(alpha(2))*data1(:,7);
staticheight=inch2m*[sind(alpha(1)),sind(alpha(1)),sind(alpha(2)),si
nd(alpha(2))].*[10.8 10.4 11.1 10.6];
Pressureatm=inch2m*[sind(alpha(1)),sind(alpha(1)),sind(alpha(2)),sin
d(alpha(2))].*[10 10 9.45 9.50];
%convert pressure heights to pressure
for i=1:4
    for j=1:27
        Pressure(j,i)=atm(i)+(Pressureatm(i)-
Pressureheight(j,i))*rhoethanol*g;
    end
end
%velocities and dynamic pressure
dynamicP=0.5*rhoair*Uinf.^2;
staticpressure=atm + (Pressureatm-staticheight)*rhoethanol*g;
%obtain uncorrected Cp(unCp)
for i=1:4
    for j=1:27
        unCp(j,i)=(Pressure(j,i)-staticpressure(i))/dynamicP(i);
    end
end
%theoretical Cp
```

```
theoCp=1-4*((sin(theta))).^2;
%uncorrectedCd by numerical integration
for i=1:4
    for j=1:27
        intergrand(j,i)=unCp(j,i)*cos(theta(j));
    end
end
uncorrectedCd=trapz(theta,intergrand);
%Apply corrections for velocity
ratio=d/h;
Ucorrect=Uinf.*(1+0.25*uncorrectedCd*ratio+0.82*(ratio^2));
%Apply corrections for Cp (correctedCp)
for i=1:4
    for j=1:27
    correctedCp(j,i)=((Uinf(i)/Ucorrect(i))^2)*(unCp(j,i)-1)+1;
    end
end
%correctedCd by numerical integration
for i=1:4
    for j=1:27
        intergrand(j,i)=correctedCp(j,i)*cos(theta(j));
    end
end
%Using the correctedCp, find the corresponding corrected Cd
correctedCd=trapz(theta,intergrand);
%Apply direct corrections for Cd (correctedCd)
DcorrectedCd=uncorrectedCd.*(1-0.5*uncorrectedCd*ratio-
2.5*(ratio^2));
%uncorrected and corrected Cl by numerical integration using
uncorrected and correctedCp
for i=1:4
    for j=1:27
        intergrand(j,i)=unCp(j,i)*sin(theta(j));
    end
end
uncorrectedCl=(trapz(theta,intergrand))/2;
for i=1:4
    for j=1:27
        intergrand(j,i)=correctedCp(j,i)*sin(theta(j));
    end
end
correctedCl=(trapz(theta,intergrand))/2;
%plot graphs
figure(1)
hold on
plot(rad2deg(theta),correctedCp(:,1),'-','LineWidth',1.2,'Color',[0,
0.4470, 0.7410]);
plot(rad2deg(theta),correctedCp(:,2),':','LineWidth',1.2,'Color',[0,
0.4470, 0.7410]);
plot(rad2deg(theta),correctedCp(:,3),'- r','LineWidth',1.2);
plot(rad2deg(theta),correctedCp(:,4),': r','LineWidth',1.2);
plot(rad2deg(theta),theoCp,'- k','LineWidth',1.5);
title('Corrected Coefficient of Pressure (Cp) vs \theta')
ylabel('Coefficient of Pressure,Cp')
xlabel('\theta, Degrees')
legend('Location','north')
```

```
legend('Tripped corrected Cp for 17.3 m/s','Untripped corrected Cp
for 18.0 m/s','Tripped corrected Cp for 37.9 m/s', 'Untripped
corrected Cp for 39.0 m/s','Theoretical distribution');
hold off

figure(2)
hold on
plot(rad2deg(theta),correctedCp(:,1),'-','LineWidth',1.2,'Color',[0,
0.4470, 0.7410]);
plot(rad2deg(theta),unCp(:,1),':','LineWidth',1.2,'Color',[0,
0.4470, 0.7410]);
plot(rad2deg(theta),correctedCp(:,2),'- r','LineWidth',1.2);
plot(rad2deg(theta),unCp(:,2),': r','LineWidth',1.2);
plot(rad2deg(theta),correctedCp(:,3),'-
','LineWidth',1.2,'Color',[0.4660, 0.6740, 0.1880]);
plot(rad2deg(theta),unCp(:,3),':','LineWidth',1.2,'Color',[0.4660,
0.6740, 0.1880]);
plot(rad2deg(theta),correctedCp(:,4),'-
','LineWidth',1.2,'Color',[0.9290, 0.6940, 0.1250]);
plot(rad2deg(theta),unCp(:,4),':','LineWidth',1.2,'Color',[0.9290,
0.6940, 0.1250]);
title('Corrected and Uncorrected Coefficient of Pressure (Cp) vs
\theta')
ylabel('Coefficient of Pressure,Cp')
xlabel('\theta, Degrees')
legend('Location','northeast')
legend('Tripped corrected Cp for 17.3 m/s','Tripped uncorrected Cp
for 16.0 m/s','Untripped corrected Cp for 18.0 m/s', 'Untripped
uncorrected Cp for 16.0 m/s','Tripped corrected Cp for 37.9
m/s','Tripped uncorrected Cp for 35.0 m/s','Untripped corrected Cp
for 39.0 m/s', 'Untripped uncorrected Cp for 35 m/s');
hold off

%Question 5 of Discussion
%Using Figure 3.44 from Figure 2 from Anatol Roshko
%work out an equivalent Reynold's Number using the Cds from t ripped
cases.
%For untripped case at 16m/s, using known test conditions
(viscosity,density), Re= 1.1 x 10*5
%For tripped case at 16m/s with a Cd=0.5563, Re=4.0*10^5
%For untripped case at 35m/s, using known test conditions
(viscosity,density), Re= 2.4 x 10*5
%For tripped case at 35m/s with a Cd=0.5900, Re=3.9*10^5


%HYPOTHETICAL CASE OF HAVING EQUAL PRESSURE DISTRIBUTION ON BOTH
HALVES OF CYLINDER
k=2;
for i=1:53
        if i<= 27
            fulltheta(i)=theta(i);
        elseif i==53
            fulltheta(i)=2*pi;
        else
            fulltheta(i)=2*pi-theta(i-k);
            k=k+2;
```

```
        end
end

for j=1:4
    k=2;
    for i=1:53
        if i<= 27
            fullcorrectedCp(i,j)=correctedCp(i,j);
        elseif i==53
            fullcorrectedCp(i,j)=correctedCp(i-52,j);
        else
            fullcorrectedCp(i,j)=correctedCp(i-k,j);
            k=k+2;
        end
    end
end

for i=1:4
    for j=1:53
        intergrand(j,i)=fullcorrectedCp(j,i)*sin(fulltheta(j));
    end
end
fullcorrectedCl=(trapz(fulltheta,intergrand))/2;
```